COMPDYN 2015
5th ECCOMAS Thematic Conference on
Computational Methods in Structural Dynamics and Earthquake Engineering
M. Papadrakakis, V. Papadopoulos, V. Plevris (eds.)
Crete Island, Greece, 25–27 May 2015

DISPERSION ANALYSIS OF ACOUSTIC WAVES IN FLUID MEDIA DISCRETIZED BY ENERGY-ORTHOGONAL FINITE ELEMENTS

Francisco José Brito Castro

Departamento de Ingeniería Industrial, Universidad de La Laguna,
Calle Méndez Núñez 67-2C, Santa Cruz de Tenerife 38001, Spain
fjbrito@ull.es

Keywords: energy-orthogonal stiffness, numerical dispersion, acoustic waves.

Abstract. *This paper studies the dispersion of acoustic waves in fluid media discretized by the finite element method. The element stiffness matrix is split into basic and higher order components which are respectively related to the mean and deviatoric components of the gradient of acoustic pressure. This decomposition is applied to the kinetic energy. The dispersion analysis yields a correlation between the higher order kinetic energy and the kinetic energy error. The use of this correlation as a reference to apply the higher order energy as an error indicator for the acoustic cavity modes computed by the finite element method is explored.*

1 INTRODUCTION

It is well known that analytical solutions to the governing equation of motion for any mechanical wave exist for just the simplest cases and only approximate solutions are feasible for the others. One method for obtaining approximate solutions is to use numerical procedures which often introduce phenomena, such as the numerical dispersion, that are not present in the physical system [1, 2].

The dispersion of acoustic waves in fluid media discretized by the finite element method is the principal topic of research in this paper. The fluid is assumed to be inviscid, compressible and homogeneous; moreover, the fluid particles oscillate in the absence of gravity and no ambient flow with small magnitude movements. The pressure and density of the fluid also undergo small perturbations respect to the ambient quantities. The resulting waves are termed linear acoustic waves. A short review of the basic theory of linear acoustic waves and the proper finite element formulation is a prerequisite in order to facilitate the subsequent developments.

1.1 Basic theory of linear acoustic waves

We consider linear acoustic waves in a fluid domain Ω with a complementary solid domain Ωs and the surface Γ representing the closed boundary of Ω and Ωs. The propagation of linear acoustic waves is described by the equation obtained by the linearization of the continuum mechanics equations of the ideal fluid [3],

$$\Delta p(\mathbf{r},t) - \frac{1}{c(\mathbf{r})^2}\frac{\partial^2 p(\mathbf{r},t)}{\partial t^2} - \nabla \ln \rho(\mathbf{r}) \cdot \nabla p(\mathbf{r},t) = 0, \quad \mathbf{r} \in \Omega \subset \mathrm{R}^3 \tag{1}$$

where: p, small perturbation of pressure or acoustic pressure; ρ, density of the fluid in the absence of acoustic wave; c, adiabatic sound velocity; t, time coordinate.

In a homogeneous medium the last term in Eq. (1) vanishes and Eq. (1) reduces to the wave equation

$$\Delta p(\mathbf{r},t) - \frac{1}{c^2}\frac{\partial^2 p(\mathbf{r},t)}{\partial t^2} = 0, \quad \mathbf{r} \in \Omega \subset \mathrm{R}^3 \tag{2}$$

For time-harmonic acoustic waves, time may be removed from the problem by writing

$$p(\mathbf{r},t) = \tilde{p}(\mathbf{r}) \exp(-i\omega t), \quad \mathbf{r} \in \Omega \subset \mathrm{R}^3 \tag{3}$$

where: $\tilde{p}(\mathbf{r})$, complex amplitude of acoustic pressure; $\omega = 2\pi / T$, circular frequency; T, period of wave.

Applying the time-harmonic dependence Eq. (3) to the wave equation Eq. (2) leads to the Helmholtz equation for the acoustic pressure

$$\Delta \tilde{p}(\mathbf{r}) + \frac{\omega^2}{c^2}\tilde{p}(\mathbf{r}) = 0, \quad \mathbf{r} \in \Omega \subset \mathrm{R}^3 \tag{4}$$

To complete a solution, the differential equation Eq. (4) requires specifying boundary conditions. Neumann boundary conditions can be assumed [4],

$$\frac{\partial \tilde{p}(\mathbf{r})}{\partial n} = \rho\omega^2 \tilde{u}_n(\mathbf{r}), \quad \mathbf{r} \in \Gamma \tag{5}$$

where: $u_n = \mathbf{u}^S \cdot \mathbf{n}$, normal component of the prescribed displacement of the boundary, $\mathbf{u}^S(\mathbf{r},t) = \tilde{\mathbf{u}}^S(\mathbf{r})\exp(-i\omega t)$; **n**, normal unit vector pointing outwards of Ω.

Dirichlet boundary conditions $\tilde{p}(\mathbf{r}) = \tilde{p}_0(\mathbf{r})$ also can be assumed.

In addition to fulfill the Helmholtz equation and the boundary conditions, solutions to scattering and radiation problems in unbounded media require that both the diffracted and radiated waves fulfill the decay condition at infinity, or Sommerfeld radiation condition [5]. In a finite computational domain different artificial boundary conditions have been proposed in order to fulfill this condition [6].

The linear acoustic waves in a homogeneous medium can be alternatively characterized by the acoustic displacement potential [3], determined by the expression

$$\mathbf{u}(\mathbf{r},t) = \nabla\psi(\mathbf{r},t), \quad \mathbf{r} \in \Omega \subset \mathrm{R}^3 \tag{6}$$

where: **u**, small displacement of the fluid particles; ψ, potential of displacement.

The relation between displacement potential and acoustic pressure will be

$$p(\mathbf{r},t) = -\rho\frac{\partial^2\psi(\mathbf{r},t)}{\partial t^2}, \quad \mathbf{r} \in \Omega \subset \mathrm{R}^3 \tag{7}$$

From Eq. (7), for time-harmonic acoustic waves, the relation between the complex amplitudes of acoustic pressure and displacement potential will be

$$\tilde{p}(\mathbf{r}) = \rho\omega^2\tilde{\psi}(\mathbf{r}), \quad \mathbf{r} \in \Omega \subset \mathrm{R}^3 \tag{8}$$

1.2 Finite element formulation

The boundary value problem Eq. (4) and (5) is posed in variational form [4]

$$\int_\Omega (\nabla p \cdot \nabla\delta p - \frac{\omega^2}{c^2}\, p\delta p)dV = \rho\omega^2\int_\Gamma (u_n\delta p)dS \tag{9}$$

The variational form Eq. (9) is discretized by the finite element method yielding the following matrix expression

$$(\mathbf{K} - \omega^2\mathbf{M})\mathbf{p} = \rho\omega^2\mathbf{\Theta}\mathbf{u}_N \tag{10}$$

where: **K**, global stiffness matrix; **M**, global mass matrix; **p,** column matrix containing the nodal values of acoustic pressure; **Θ**, boundary mass matrix; $\mathbf{u}_N$, column matrix containing the nodal values of the prescribed normal displacement of the boundary.

Defining at element level the matrix $\mathbf{B}^e$ relating the gradient of acoustic pressure to the nodal values of acoustic pressure,

$$\nabla p^e = \mathbf{B}^e\mathbf{p}^e \tag{11}$$

the element stiffness matrix is then written $\mathbf{K}^e = \int_{\Omega e}(\mathbf{B}^e)^T\mathbf{B}^e dV$.

The acoustic kinetic energy of the fluid occupying the bounded domain Ω will be

$$E_{ko} = \frac{1}{2\rho\omega^2}\int_\Omega \mathrm{Re}[i\nabla p]\cdot\mathrm{Re}[i\nabla p]dV \tag{12}$$

For the discretized domain, inserting Eq. (11) into Eq. (12) at element level, the element acoustic kinetic energy is yielded. The kinetic energy of the finite element assemblage will be the sum of the element energies. Then,

$$E_k = \frac{1}{2\rho\omega^2} \mathrm{Re}[i(\mathbf{p})^T] \mathbf{K} \mathrm{Re}[i\mathbf{p}] \tag{13}$$

1.2.1 Energy-orthogonal decomposition

The matrix relating the gradient of acoustic pressure to the nodal values of acoustic pressure at element level Eq. (11) is partitioned into mean and deviatoric components, $\mathbf{B}^e = \overline{\mathbf{B}}^e + \mathbf{B}_d^e$, where $\overline{\mathbf{B}}^e V^e = \int_{\Omega e} \mathbf{B}^e dV$ and $\mathbf{B}_d^e = \mathbf{B}^e - \overline{\mathbf{B}}^e$.

The element stiffness matrix is then written

$$\mathbf{K}^e = \mathbf{K}_b^e + \mathbf{K}_h^e \tag{14}$$

where: $\mathbf{K}_b^e = \int_{\Omega e} (\overline{\mathbf{B}}^e)^T \overline{\mathbf{B}}^e dV$, basic stiffness matrix; $\mathbf{K}_h^e = \int_{\Omega e} (\mathbf{B}_d^e)^T \mathbf{B}_d^e dV$, higher order stiffness matrix.

In this case it is said that the element stiffness matrix is decomposed in energy-orthogonal form [7]. The concept of energy-orthogonal stiffness matrix regarded in this paper was explicitly introduced in the context of the linear elasticity by Bergan and Nygärd within the framework of the Free Formulation [8], and by Felippa within the framework of the Parametrized Variational Principles [9].

The decomposition in Eq. (14) holds for the complete model whenever $\mathbf{K}_b^e$ and $\mathbf{K}_h^e$ are independently assembled,

$$\mathbf{K} = \mathbf{K}_b + \mathbf{K}_h \tag{15}$$

Inserting Eq. (15) into Eq. (13), we obtain the basic and higher order acoustic kinetic energies of the finite element assemblage.

1.2.2 Stationary waves

For a stationary wave, the amplitude of the acoustic pressure is a real-valued function. Then, from Eq. (13), the period-averaged acoustic kinetic energy of the fluid for the discretized domain will be

$$\overline{E}_k = \frac{1}{2\rho\omega^2} \tilde{\mathbf{p}}^T \mathbf{K} \tilde{\mathbf{p}} \int_0^1 \sin^2(2\pi\tau) d\tau$$

$$\overline{E}_k = \frac{1}{4\rho\omega^2} \tilde{\mathbf{p}}^T \mathbf{K} \tilde{\mathbf{p}} \tag{16}$$

where: $\tau = t/T$, $0 \le \tau \le 1$, dimensionless time; $\tilde{\mathbf{p}}$, column matrix containing the real nodal amplitudes of the acoustic pressure.

1.3 Scope of research

In this paper the dispersion properties and the density of period-averaged kinetic energy are computed for plane harmonic waves in unbounded media discretized by regular meshes of energy-orthogonal finite elements. Given the mesh, in the limit of

long wavelength, although the kinetic energy density does not vanish, its higher order component does vanish. Similarly, given the wavelength, as the solution converges on account of mesh refinement, the kinetic energy density is increasingly dominated by its basic component. The above heuristic argument motivates to research the relationship between the higher order kinetic energy and the discretization error in order to explore the behaviour of this energy component as an error indicator. To be precise, by the dispersion analysis, a correlation between the percentage of higher order kinetic energy and the kinetic energy error will be yielded. The use of this correlation as a reference to apply the higher order kinetic energy as an error indicator for the acoustic modes computed by the finite element method will be explored. A similar correlation has been proposed for linear gravity waves in fluid media [10]. Arguments to support the higher order energy as an error indicator have been established in the context of the linear elasticity [9].

2 DISPERSION ANALYSIS

2.1 Characteristic equations

The unbounded fluid domain is discretized by a regular mesh of finite elements. Three different isoparametric finite elements are considered: the hexahedron with twenty nodes and brick geometry HE20, Fig. 1, the pentahedron with fifteen nodes and right prismatic isosceles geometry PE15, Fig. 2, and the tetrahedron with ten nodes TE10. The mesh with TE10 elements is formed by dividing the unbounded domain in bricks with twenty seven nodes and then dividing each brick into six tetrahedrons [11], Fig. 3. The nodal lattice formed by the finite element assemblage has four, five and eight nodes per unit cell, respectively. Different meshes with the same element volume are yielded by selecting the aspect ratio parameter, where $0 < \gamma \leq 1$; additionally, for the HE20 and TE10 meshes, the skew angle also can be selected, where $0 \leq \beta < 90º$. The finite element analysis will be performed by using the rectangular coordinate system XYZ.

For an uniform plane harmonic wave propagating in the unbounded fluid domain,

$$\tilde{p}(\mathbf{r}) = A\exp(i\kappa\mathbf{n}\cdot\mathbf{r}) \tag{17}$$

where: A, wave amplitude; $\mathbf{n}$, wave normal, unit vector indicating the direction of wave propagation; $\kappa = \omega/c = 2\pi/\lambda$, wave number; λ, wavelength.

The wave normal has the components, Fig. 4,

$$\mathbf{n} = (\cos\phi\sin\theta, \sin\phi\sin\theta, \cos\theta) \tag{18}$$

where: ϕ, $0 \leq \phi \leq 180º$, azimuthal angle; θ, $0 \leq \theta \leq 180º$, polar angle.

For the plane acoustic wave Eq. (17) the density of period-averaged kinetic energy can be computed by the equation [12]

$$\overline{E}_{ko} = \frac{A^2}{4\rho c^2} \tag{19}$$

The characteristic equations can be found assuming harmonic waves Eq. (17) with different amplitudes in each node of the unit cell,

$$\tilde{p} = A_j \exp(i\kappa\mathbf{n}\cdot\mathbf{r}), \quad j = 1,\ldots,N \tag{20}$$

where: N, number of nodes per unit cell.

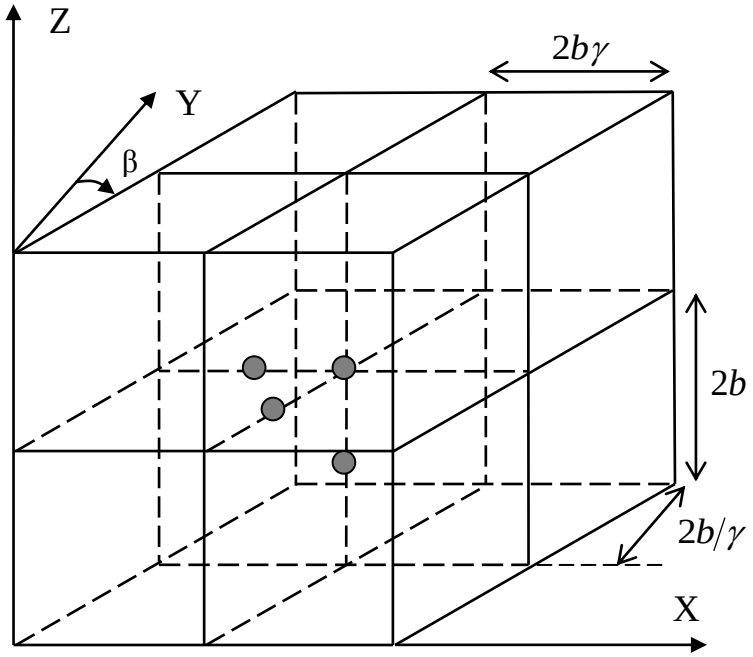

Figure 1: Regular mesh of twenty-nodes hexahedral elements and unit cell.

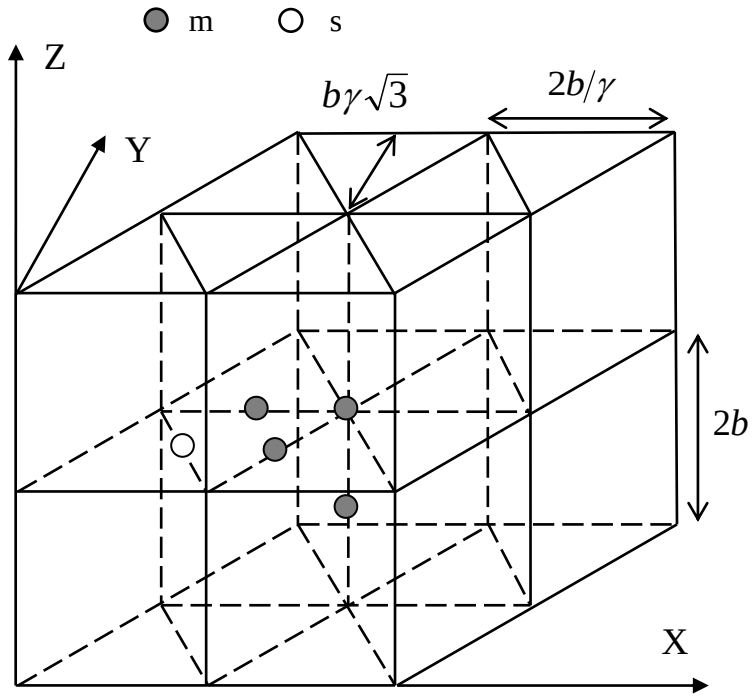

Figure 2: Regular mesh of fifteen-nodes pentahedral elements and unit cell.

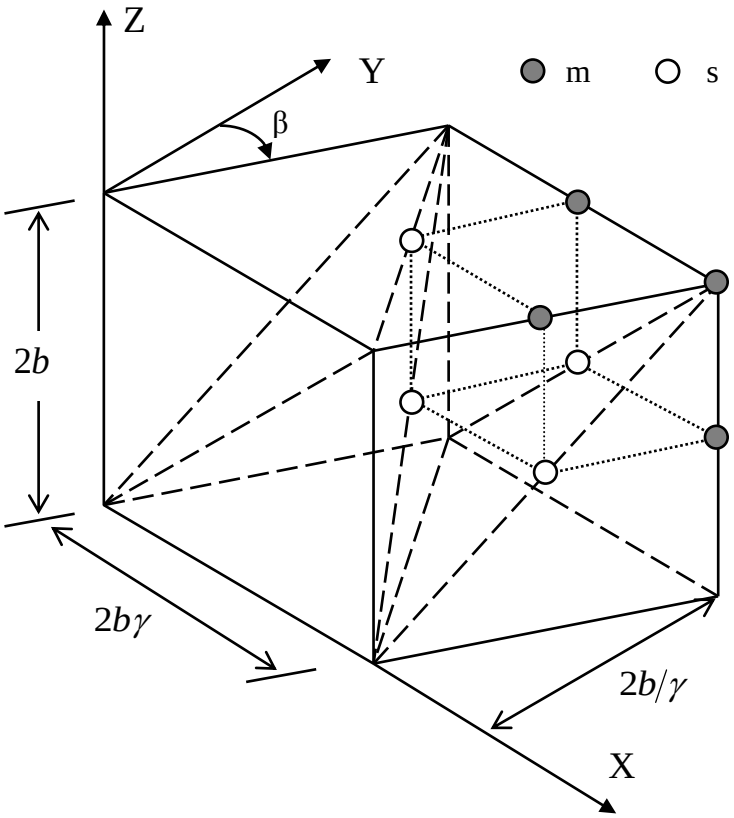

Figure 3: Regular mesh of ten-nodes tetrahedral elements and unit cell.

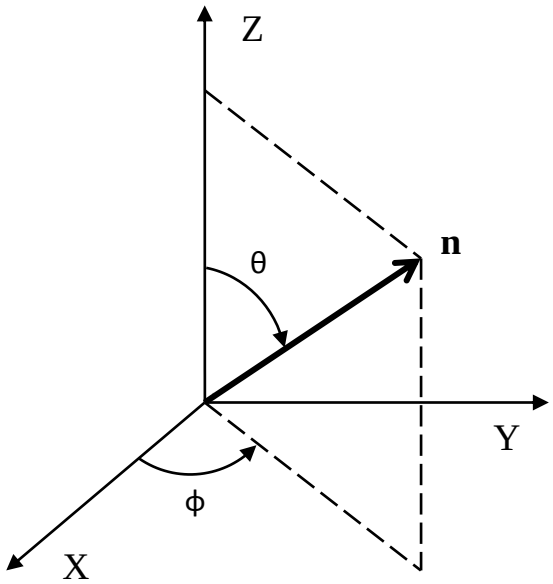

Figure 4: Unit vector indicating the direction of wave propagation.

Inserting the solutions Eq. (20) into the homogeneous part of Eq. (10), the characteristic equation for each node of the unit cell is yielded by equilibrium of generalized nodal forces [13]. A homogeneous system of N algebraic equations is formed,

$$\begin{gathered}\mathbf{ZA}=\mathbf{0}\\ z_{ij}A_j=0,\quad i,j=1,\ldots,N\end{gathered} \tag{21}$$

$$z_{ij}=a_{ij}(m,\phi,\theta,\boldsymbol{\varepsilon})+\varpi^2 b_{ij}(m,\phi,\theta,\boldsymbol{\varepsilon}) \tag{22}$$

$$m=\frac{b\kappa}{\pi}=\frac{2b}{\lambda},\quad \varpi=\frac{2b}{c}\omega \tag{23}$$

where: m, dimensionless wave number, $0 < m < 1$; b, half of the element size; ϖ, dimensionless frequency of the discretized fluid domain; $\boldsymbol{\varepsilon}=(\gamma,\beta)$ form parameters for HE20 and TE10 meshes, or $\boldsymbol{\varepsilon}=(\gamma)$ form parameter for PE15 mesh.

2.2 Dispersion equations

The system of homogeneous algebraic equations given in Eq. (21) has a non-trivial solution only if the matrix $\mathbf{Z}$ is singular; that is,

$$\det\left[\mathbf{Z}(m,\phi,\theta,\boldsymbol{\varepsilon},\varpi)\right]=0 \tag{24}$$

From Eq. (24) the following polynomial equation is yielded

$$\sum_{r=0}^{N} c_r q^r=0,\quad c_N=1 \tag{25}$$

where: $q=\varpi^2$; $c_r(m,\phi,\theta,\boldsymbol{\varepsilon})$, coefficients obtained from a_{ij} and b_{ij}, Eq. (22).

Either of Eq. (24) and (25) is called a characteristic frequency equation for the plane wave propagation.

It is an important fact that the N zeroes of a polynomial of degree $N \geq 1$ with complex coefficients depend continuously upon the coefficients [14]. Thus, sufficiently small changes in the coefficients of a polynomial can lead only to small changes in any zero. However, if the zeros are numerically computed, there is no simple way to define a function which takes the N coefficients (all but the leading 1) of a monic polynomial of degree N to the N zeroes of the polynomial, since there is no natural way to define an ordering among the N zeroes. In the case of the HE20 mesh, for which the polynomial Eq. (25) is quartic, the above difficulty has been overcome by computing the zeroes in closed form as functions of its coefficients. Then, the components

$$q_k=q_k(c_0,\ldots,c_3),\ k=1,\ldots,4 \tag{26}$$

or, alternatively,

$$\varpi_k=\varpi_k(m,\phi,\theta,\boldsymbol{\varepsilon}),\quad k=1,\ldots,4 \tag{27}$$

will be continuous functions precisely defined. They are called dispersion equations. Obviously, we suppose that the coefficients $c_r(m,\phi,\theta,\boldsymbol{\varepsilon})$ are also continuous functions.

Substituting Eq. (27) into Eq. (21), the wave amplitudes corresponding to the nodes of the unit cell for the HE20 mesh are yielded for each dispersion equation. In this work,

each set of linear algebraic equations is numerically solved by using the singular value decomposition method SVD [15].

To find the zeros of a polynomial equation as functions of its coefficients beyond the quartic equation is a very difficult mathematical problem [16]. Then, for the meshes PE15 and TE10 which have five and eight nodes per unit cell, respectively, if the zeros of Eq. (25) are numerically computed, the above mentioned ordering difficulty could be a problem. In this case, by considering the initial condition,

$$\lim_{m\to 0} \varpi_1(\phi,\theta,\boldsymbol{\varepsilon}) = 0 \tag{28}$$

we propose to compute the first dispersion equation by a reduced unit cell obtained by a procedure of exact dynamic condensation [17].

Assume that the total nodes at the unit cell are categorized as master nodes (m) and slave nodes (s), where the number of master nodes is four, and the number of slave nodes is one and four for P15 and TE10 meshes, respectively, see Fig. 2 and 3. With this arrangement, the system of characteristic equations Eq. (21) may be partitioned as

$$\begin{pmatrix} \mathbf{Z}_{mm} & \mathbf{Z}_{ms} \\ \mathbf{Z}_{sm} & \mathbf{Z}_{ss} \end{pmatrix} \begin{pmatrix} \mathbf{A}_m \\ \mathbf{A}_s \end{pmatrix} = \begin{pmatrix} \mathbf{0} \\ \mathbf{0} \end{pmatrix} \tag{29}$$

where:

$$\begin{aligned} \mathbf{Z}_{mm} &= \mathbf{a}_{mm} + q\mathbf{b}_{mm}, \quad \mathbf{Z}_{ms} = \mathbf{a}_{ms} + q\mathbf{b}_{ms} \\ \mathbf{Z}_{sm} &= \mathbf{a}_{sm} + q\mathbf{b}_{sm}, \quad \mathbf{Z}_{ss} = \mathbf{a}_{ss} + q\mathbf{b}_{ss} \end{aligned} \tag{30}$$

The relation of wave amplitudes between the master and slave nodes may be obtained from Eq. (29) as

$$\mathbf{A}_s = -\mathbf{Z}_{ss}^{-1}(q)\mathbf{Z}_{sm}(q)\mathbf{A}_m \tag{31}$$

Then, by back-substituting, the system of characteristic equations of the reduced unit cell is obtained as

$$\begin{aligned} \mathbf{Z}_R(q)\mathbf{A}_m &= \mathbf{0} \\ (\mathbf{K}_R(q) + q\mathbf{M}_R(q))\mathbf{A}_m &= \mathbf{0} \end{aligned} \tag{32}$$

where:

$$\begin{aligned} \mathbf{K}_R(q) &= \mathbf{a}_{mm} - \mathbf{Z}_{ms}\mathbf{Z}_{ss}^{-1}\mathbf{a}_{sm} + \mathbf{Z}_{ms}\mathbf{Z}_{ss}^{-1}\mathbf{a}_{ss}\mathbf{Z}_{ss}^{-1}\mathbf{Z}_{sm} - \mathbf{a}_{ms}\mathbf{Z}_{ss}^{-1}\mathbf{Z}_{sm} \\ \mathbf{M}_R(q) &= \mathbf{b}_{mm} - \mathbf{Z}_{ms}\mathbf{Z}_{ss}^{-1}\mathbf{b}_{sm} + \mathbf{Z}_{ms}\mathbf{Z}_{ss}^{-1}\mathbf{b}_{ss}\mathbf{Z}_{ss}^{-1}\mathbf{Z}_{sm} - \mathbf{b}_{ms}\mathbf{Z}_{ss}^{-1}\mathbf{Z}_{sm} \end{aligned} \tag{33}$$

Then, from Eq. (32), the reduced form of the characteristic frequency equation is obtained

$$\begin{aligned} q^4 + c_{3R}q^3 + c_{2R}q^2 + c_{1R}q + c_{0R} &= 0 \\ c_{rR}(m,\phi,\theta,\boldsymbol{\varepsilon},q), \quad r &= 0,\ldots,3 \end{aligned} \tag{34}$$

The first dispersion equation is computed by the following iterative procedure:
Set by Eq. (28) the initial value $q_{i1} = 0$.

Do for $0 < m < 1$, step Δm

1. Compute the coefficients $c_{rR}(m,\phi,\theta,\boldsymbol{\varepsilon},q_{i1})$ of Eq. (34).

2. Compute the zero q_1 of the quartic polynomial Eq. (34).

Do while ($\left|\frac{q_1 - q_{i1}}{q_1}\right| \geq \delta$)

1. Refresh initial value $q_{i1} = q_1$.
2. Compute the coefficients $c_{rR}(m, \phi, \theta, \boldsymbol{\varepsilon}, q_{i1})$ of Eq. (34).
3. Compute the zero q_1 of the quartic polynomial Eq. (34).

End do

3. Substituting q_1 into Eq. (32) to compute the wave amplitudes at the master nodes.
4. Substituting q_1 into Eq. (31) to compute the wave amplitudes at the slave nodes.
5. Refresh initial value $q_{i1} = q_1$ for the next step.

End do

The range of dimensionless wave number values where each dispersion equation represents the propagation of acoustic waves in the discretized medium will be called the acoustical branch of the dispersion equation. In order to determine the acoustical branches, a preliminary constraint condition over the dimension of the null space of **Z** for the H20 mesh, or $\mathbf{Z}_R$ for PE15 and TE10 meshes, must be imposed,

$$\dim[\mathbf{N}(\mathbf{Z})] = 1 \quad or \quad \dim[\mathbf{N}(\mathbf{Z}_R)] = 1 \tag{35}$$

The constraint condition Eq. (35) implies that the subspace of solutions to Eq. (21) or Eq. (32) must be one-dimensional. In this case the vector of wave amplitudes **A** or $\mathbf{A}_\mathrm{m}$ is arbitrary to the extent that a scalar multiple of it is also a solution. Then the following constraint conditions are imposed,

$$A_1 = 1, \quad \begin{cases} A_2(m, \phi, \theta, \boldsymbol{\varepsilon}) > 0 \\ A_3(m, \phi, \theta, \boldsymbol{\varepsilon}) > 0 \\ A_4(m, \phi, \theta, \boldsymbol{\varepsilon}) > 0 \end{cases} \tag{36}$$

$$\left(\frac{\partial \varpi}{\partial m}\right)_{\phi, \theta, \boldsymbol{\varepsilon}} > 0 \tag{37}$$

In molecular physics, condition Eq. (36) is called the restriction of the lattice spectrum to the acoustical branch [18]. Obviously, if the constraint condition Eq. (35) is not imposed, the constraint condition Eq. (36) is meaningless.

From Eq. (23) we obtain both the phase velocity and group velocity of the discretized medium,

$$c_d = \frac{c}{2\pi} \frac{\varpi}{m} \tag{38}$$

$$c_{g,d} = \frac{\partial \omega}{\partial \kappa} = \frac{c_g}{2\pi} \frac{\partial \varpi}{\partial m} \tag{39}$$

where: c, phase velocity of the continuum (adiabatic sound velocity) ; c_g , group velocity of the continuum.

From Eq. (39), the constraint condition Eq. (37) is equivalent to

$$c_{g,d} > 0 \tag{40}$$

It can be proven that for general periodic motion the energy propagates with the group velocity [19]; therefore, the constraint condition Eq. (40) imposes that the energy propagates into the wave direction. From this point, for each dispersion equation only the acoustical branch will be considered. This one represents the physically admissible solution for mechanical wave propagation.

It must be recall that the group velocity of the continuum will be equal to the phase velocity because the waves propagate non-dispersively. Nevertheless, for the dispersive discretized medium the group velocity will be different from the phase velocity; therefore, the velocity of energy transport will be different from the phase velocity. As a consequence, when we consider the numerical dispersion associated with the finite element spatial discretization, not only the effect over the phase velocity must be analyzed but also the effect over the group velocity or velocity of energy transport.

2.3 Kinetic energy at the unit cell

For a fluid domain discretized by a regular mesh of finite elements, the stiffness matrix can be expressed in the suitable form $\mathbf{K} = (2b)\mathbf{K}^0$. Then, from Eq. (13) and (23), the kinetic energy at the unit cell over a period will be

$$E_k = \frac{1}{2\rho c^2 \varpi^2}(2b)^3 \,\mathrm{Re}[i(\tilde{\mathbf{p}})^T \exp(-i2\pi\tau)]\,\mathrm{Re}[i\tilde{\mathbf{G}}^0 \exp(-i2\pi\tau)] \tag{41}$$

where: $\mathbf{G}^0 = \tilde{\mathbf{G}}^0 \exp(-i2\pi\tau)$, column matrix of generalized forces at the nodes of the unit cell, obtained from the stiffness matrix $\mathbf{K}^0$.

From Eq. (41), the density of period-averaged kinetic energy is computed,

$$\overline{E}_k = \frac{C}{2\rho c^2 \varpi^2}\int_0^1 \mathrm{Re}[i(\tilde{\mathbf{p}})^T \exp(-i2\pi\tau)]\,\mathrm{Re}[i\tilde{\mathbf{G}}^0 \exp(-i2\pi\tau)]d\tau \tag{42}$$

where: $C = 1$, for HE20 and TE10 meshes; $C = 2/\sqrt{3}$, for PE15 mesh.

From the decomposition in Eq. (15), $\mathbf{K}^0 = \mathbf{K}_b^0 + \mathbf{K}_h^0$, the density of period-averaged kinetic energy Eq. (42) can be partitioned as addition of basic and higher order components. The latter component will be

$$\overline{E}_{kh} = \frac{C}{2\rho c^2 \varpi^2}\int_0^1 \mathrm{Re}[i(\tilde{\mathbf{p}})^T \exp(-i2\pi\tau)]\,\mathrm{Re}[i\tilde{\mathbf{G}}_h^0 \exp(-i2\pi\tau)]d\tau \tag{43}$$

where: $\mathbf{G}_h^0 = \tilde{\mathbf{G}}_h^0 \exp(-i2\pi\tau)$, column matrix of higher order generalized forces at the nodes of the unit cell, obtained from the higher order stiffness matrix $\mathbf{K}_h^0$.

From Eq. (43) and (42), the percentage of period-averaged higher order kinetic energy can be defined as

$$e_h = \frac{\overline{E}_{kh}}{\overline{E}_k}, \quad e_h = e_h(m, \phi, \theta, \boldsymbol{\varepsilon}) \tag{44}$$

2.4 Indicators of discretization error

By considering Eq. (38) and (39), the indicators of the dispersion associated with spatial discretization that is introduced by the finite element model are defined as

$$e_d = \frac{c_d}{c} = \frac{\varpi}{2m\pi}, \quad e_d = e_d(m, \phi, \theta, \boldsymbol{\varepsilon}) \tag{45}$$

$$e_{g,d} = \frac{c_{g,d}}{c_g} = \frac{1}{2\pi}\frac{\partial \varpi}{\partial m}, \quad e_{g,d} = e_{g,d}(m, \phi, \theta, \boldsymbol{\varepsilon}) \tag{46}$$

These indicators consider the effect of the spatial discretization over the wave velocity and the velocity of energy transport, respectively.

From Eq. (42) and (19), the indicator of kinetic energy error associated with spatial discretization that is introduced by the finite element model is defined as

$$e_k = \frac{\overline{E}_k}{\overline{E}_{ko}}, \quad e_k = e_k(m, \phi, \theta, \boldsymbol{\varepsilon}) \tag{47}$$

Alternatively, the percentage of kinetic energy error can be defined as

$$\varepsilon_k = e_k - 1, \quad \varepsilon_k = \varepsilon_k(m, \phi, \theta, \boldsymbol{\varepsilon}) \tag{48}$$

2.5 Numerical research

Three different meshes having the same element volume will be considered for each of the analyzed elements. Specifically, for HE20 and TE10 elements, Fig. 1 and 3:

Q1; square section, $\gamma = 1, \quad \beta = 0$

Q2; rectangular section with aspect ratio 1:2, $\gamma = \frac{1}{\sqrt{2}}, \quad \beta = 0$

Q3; skewed section, $\gamma = 1, \quad \beta = 45^{\circ}$

and, for PE15 element, Fig. 2:

Q1; triangular section of equilateral geometry, $\gamma = 1$

Q2; triangular section of right geometry, $\gamma^2 = \frac{1}{\sqrt{3}}$

Q3; triangular section with angle of 30º opposite to the base, $\gamma^2 = \frac{\tan 75^{\circ}}{\sqrt{3}}$

The indicators Eq. (44) to (48) are computed versus dimensionless wave number for different directions of wave propagation.

For the mesh HE20-Q3, the indicator of dispersion Eq. (45) is plotted in Fig. 5. Given the azimuthal angle ϕ, three values of the polar angle θ are considered in order to represent the anisotropy induced by the spatial discretization. The numerical dispersion is clearly displayed as the dimensionless wave number increases. A discontinuity in phase velocity is observed around $m = 1/2$ for $\theta = 0^{\circ}$. In this case the discretized fluid domain acts like a band-pass filter [13]. This discontinuity was already described by Brillouin [18] for lattices consisting of different particles.

For the mesh Q1 and a selected direction of wave propagation the indicators Eq. (47) and Eq. (44) are plotted versus dimensionless wave number for each of the considered elements, Fig. 6 and 7. It is observed that the kinetic energy error vanishes both as the mesh is refined and in the limit of long wavelength, as it is expected. Similarly, the density of higher order kinetic energy also vanishes both as the mesh is refined and in the limit of long wavelength. This latter behaviour also is expected because the acoustic

pressure field inside each element becomes uniform. As a conclusion, the dispersion analysis reveals that the higher order kinetic energy behaves as an error indicator.

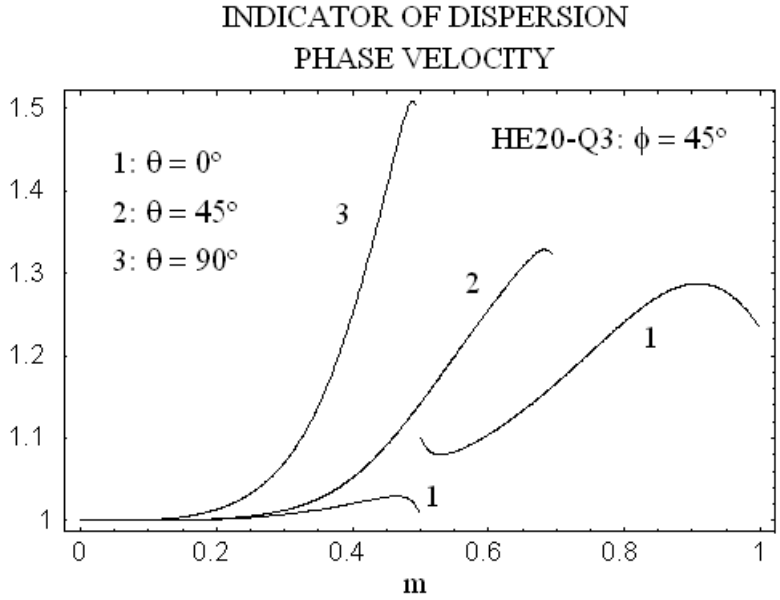

Figure 5: Indicator of dispersion associated with the phase velocity versus dimensionless wave number.

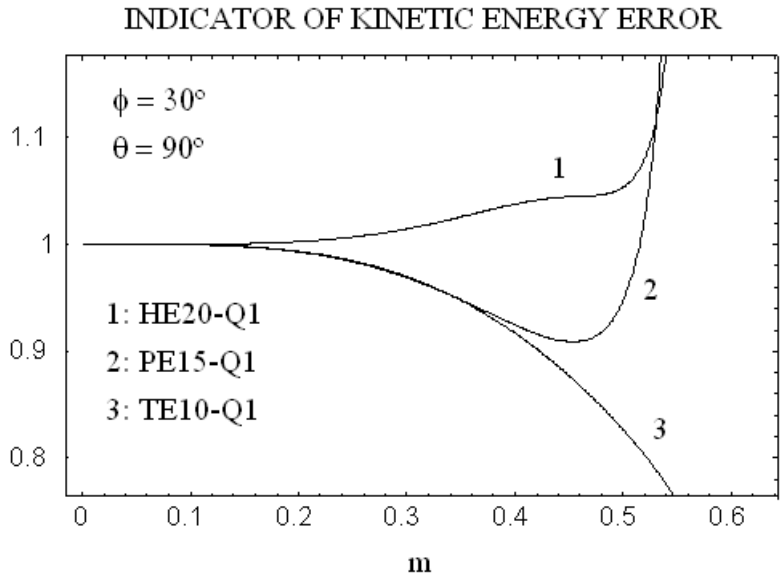

Figure 6: Indicator of kinetic energy error versus dimensionless wave number.

In order to explore the behaviour of the higher order kinetic energy as an error indicator, a correlation between the percentage of higher order kinetic energy and the kinetic energy error is pursued. As a first step, from Eq. (44) and (48), a mapping that associates a value of percentage of kinetic energy error to each value of percentage of higher order kinetic energy is defined,

$$\varepsilon_k = \varepsilon_k(e_h, \phi, \theta, \boldsymbol{\varepsilon}) \tag{49}$$

For the mesh Q1 and a selected direction of wave propagation the mapping Eq. (49) is plotted in Fig. 8 for each of the considered elements. It is observed that in each case, and for moderate values of percentage of higher order kinetic energy, this mapping could be approximated by the following cubic correlation,

$$\varepsilon_k = (A * e_h + B) * e_h^2 \tag{50}$$

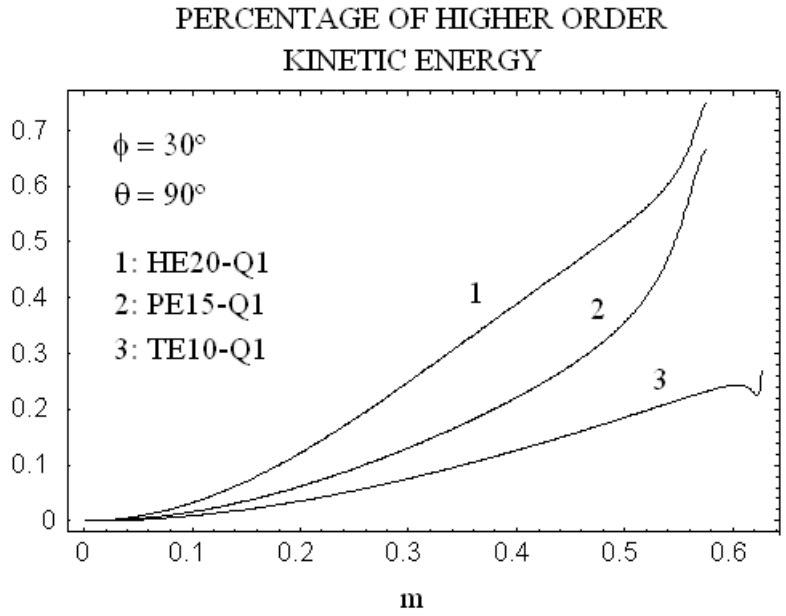

Figure 7: Percentage of higher order kinetic energy versus dimensionless wave number.

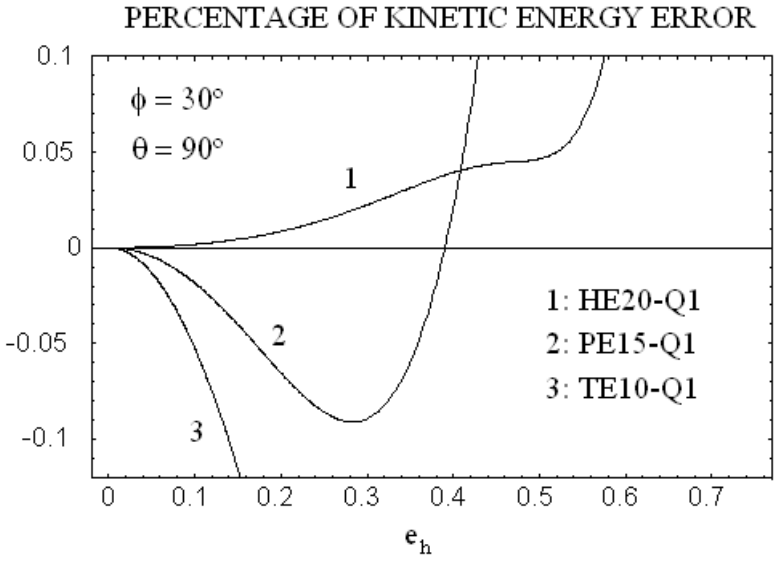

Figure 8: Percentage of kinetic energy error versus percentage of higher order kinetic energy.

As a second step, for each of the considered elements, two values of percentage of higher order kinetic energy Eq. (44) are selected as reference ones,

$$HE20: \quad e_{h1} = 0.10 \quad e_{h2} = 0.20 \tag{51}$$

$$PE15: \quad e_{h1} = 0.075 \quad e_{h2} = 0.15 \tag{52}$$

$$TE10: \quad e_{h1} = 0.03 \quad e_{h2} = 0.06 \tag{53}$$

From Eq. (44) and Eq. (51) to (53), the first and the second reference dimensionless wave number are defined for each of the considered elements,

$$m_1 = f_{m1}(\phi, \theta, \boldsymbol{\varepsilon}) \tag{54}$$

$$m_2 = f_{m2}(\phi, \theta, \boldsymbol{\varepsilon}) \tag{55}$$

As a third step, from Eq. (48) and (54), and from Eq. (48) and (55), the first and the second reference values of percentage of kinetic energy error are defined,

$$\varepsilon_{k1} = f_{k1}(\phi, \theta, \boldsymbol{\varepsilon}) \tag{56}$$

$$\varepsilon_{k2} = f_{k2}(\phi, \theta, \boldsymbol{\varepsilon}) \tag{57}$$

Similar reference values can be defined for the indicator of dispersion associated with the group velocity,

$$e_{g1} = f_{g1}(\phi, \theta, \boldsymbol{\varepsilon}) \tag{58}$$

$$e_{g2} = f_{g2}(\phi, \theta, \boldsymbol{\varepsilon}) \tag{59}$$

For the element TE10 and the mesh Q3, Eq. (55), (57) and (59) are displayed versus polar angle θ for selected values of azimuthal angle ϕ, Fig. 9 to 11.

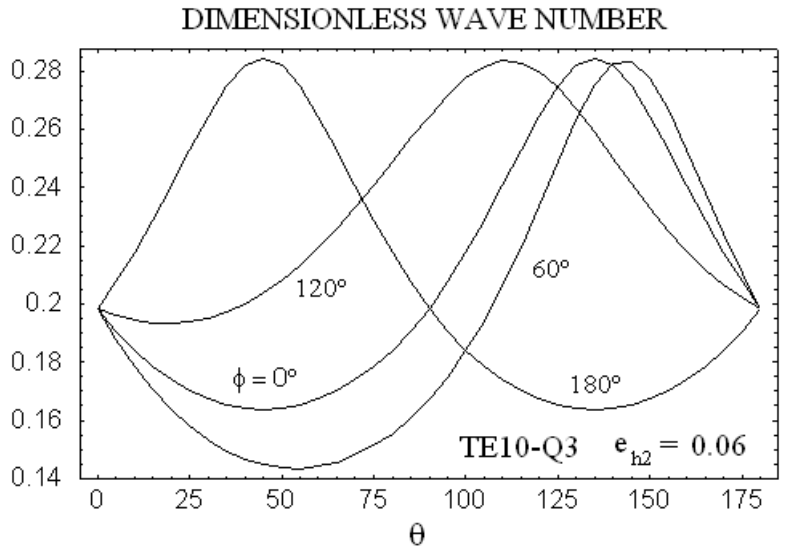

Figure 9: Second reference value of dimensionless wave number versus the polar angle.

As a fourth step, for each of the considered elements, the root-mean-square value and the maximum absolute value of Eq. (56) and (57) are computed over the range of azimuthal and polar angles. The results are shown in Tables 1 to 3. Also, the mean values of Eq. (54) and (55), and the mean values of Eq. (58) and (59), are computed.

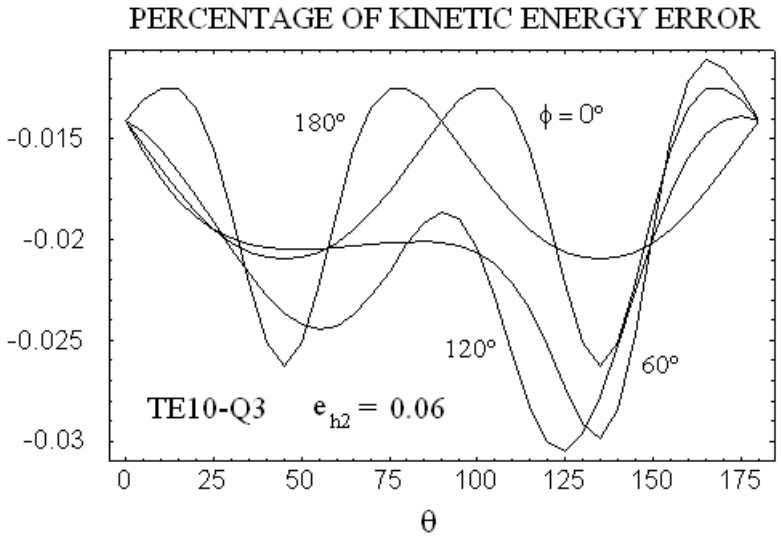

Figure 10: Second reference value of percentage of kinetic energy error versus the polar angle.

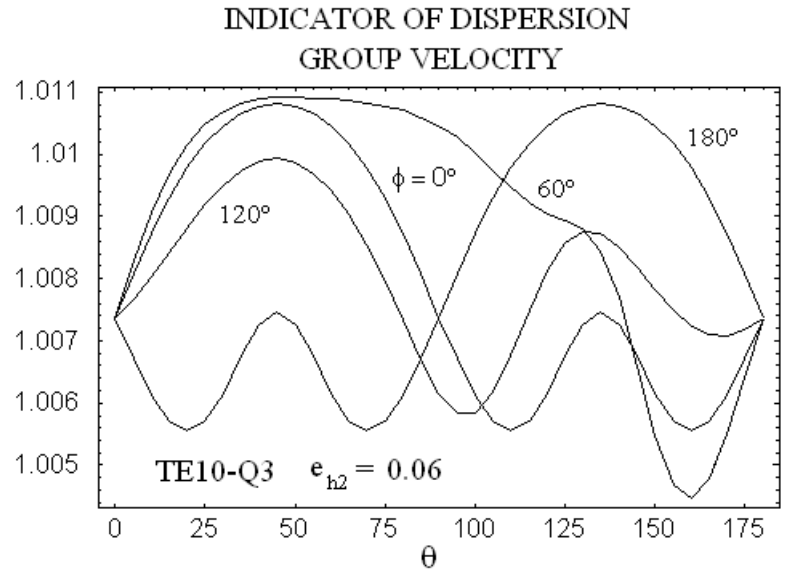

Figure 11: Second reference value of indicator of dispersion associated with the group velocity versus the polar angle.

As a last step, for each of the considered elements, we propose to apply the cubic correlation Eq. (50) to define a mapping that associates a standard value of percentage of kinetic energy error to each value of percentage of higher order kinetic energy. The coefficients *A* and *B* are solved using the averaging of root-mean-square values computed for Eq. (56) and (57), Tables 1 to 3. Specifically,

$$\varepsilon_k^{HE20} = (0.416000 * e_h + 0.273100) * e_h^2, \quad 0 < e_h \leq 0.20 \tag{60}$$

$$\varepsilon_k^{PE15} = (0.337185 * e_h + 0.828222) * e_h^2, \quad 0 < e_h \leq 0.15 \tag{61}$$

$$\varepsilon_k^{TE10} = (2.722222 * e_h + 5.856111) * e_h^2, \quad 0 < e_h \leq 0.06 \tag{62}$$

In Fig. 12 the standard correlations Eq. (60) to (62) are displayed. In each case the interval of application can be moderately extended beyond the upper limit of percentage of higher order kinetic energy used to compute the coefficients *A* and *B*. It is observed that the correlation between standard percentage of kinetic energy error and percentage of higher order kinetic energy is highly dependent of the considered element. The correlation for PE15 element is between the ones for TE10 and HE20 elements, as it could be expected.

HE20				
$e_{h1} = 0.10$	ε_{k1}^{RMS}	ε_{k1}^{MAX}	$\overline{m}_1$	$\overline{e}_{g1}$
MESH Q1	0.003279	0.006283	0.1797	1.002710
MESH Q2	0.003126	0.006151	0.1752	1.002680
MESH Q3	0.003035	0.008281	0.1711	1.003330
Averaged value	0.003147	0.006905	0.1753	1.002907
$e_{h2} = 0.20$	ε_{k2}^{RMS}	ε_{k2}^{MAX}	$\overline{m}_2$	$\overline{e}_{g2}$
MESH Q1	0.014991	0.030342	0.2627	1.011810
MESH Q2	0.013883	0.029227	0.2561	1.011680
MESH Q3	0.013882	0.041620	0.2500	1.014770
Averaged value	0.014252	0.033730	0.2563	1.012753

Table 1: Characteristic reference values for HE20 element over the range of azimuthal and polar angles.

PE15				
$e_{h1} = 0.075$	ε_{k1}^{RMS}	ε_{k1}^{MAX}	$\overline{m}_1$	$\overline{e}_{g1}$
MESH Q1	0.004139	0.010875	0.1833	1.002700
MESH Q2	0.004900	0.017457	0.1805	1.002990
MESH Q3	0.005365	0.020527	0.1779	1.002900
Averaged value	0.004801	0.016286	0.1806	1.002863
$e_{h2} = 0.15$	ε_{k2}^{RMS}	ε_{k2}^{MAX}	$\overline{m}_2$	$\overline{e}_{g2}$
MESH Q1	0.016810	0.045641	0.2667	1.011470
MESH Q2	0.020345	0.076963	0.2627	1.012680
MESH Q3	0.022165	0.084933	0.2589	1.012340
Averaged value	0.019773	0.069179	0.2628	1.012163

Table 2: Characteristic reference values for PE15 element over the range of azimuthal and polar angles.

Also, for each of the considered elements, we propose to apply a quadratic correlation to define a mapping that associates a mean value of dimensionless wave number to each value of percentage of higher order kinetic energy,

$$\overline{m} = (A * e_h + B) * e_h, \quad 0 < e_h \leq e_{h2} \tag{63}$$

The coefficients *A* and *B* are solved using the averaging of mean dimensionless wave number computed for Eq. (54) and (55), Tables 1 to 3. The correlation Eq. (63) is

displayed in Fig. 13. For a particular mesh and direction of wave propagation, in Fig. 7 the quadratic dependence between dimensionless wave number and percentage of higher order kinetic energy can be observed is approximately fulfilled for each of the considered elements in the interested range of percentage of higher order kinetic energy.

TE10				
$e_{h1} = 0.03$	ε_{k1}^{RMS}	ε_{k1}^{MAX}	$\overline{m}_1$	$\overline{e}_{g1}$
MESH Q1	0.005607	0.009749	0.1454	1.002380
MESH Q2	0.005479	0.010164	0.1423	1.002160
MESH Q3	0.004946	0.007412	0.1471	1.002060
Averaged value	0.005344	0.009108	0.1449	1.002200
$e_{h2} = 0.06$	ε_{k2}^{RMS}	ε_{k2}^{MAX}	$\overline{m}_2$	$\overline{e}_{g2}$
MESH Q1	0.022668	0.041343	0.2100	1.009610
MESH Q2	0.022113	0.040651	0.2056	1.008740
MESH Q3	0.020229	0.030939	0.2125	1.008370
Averaged value	0.021670	0.037644	0.2094	1.008907

Table 3: Characteristic reference values for TE10 element over the range of azimuthal and polar angles.

2.6 Remark

It is clear that the harmonic acoustic waves cannot be exactly captured by a regular mesh of finite elements HE20, PE15 or TE10. This fact is a consequence of the element interpolation which is quadratic. A substitute wave field [20] or alias field [21] has been obtained in the discretized unbounded medium by performing a dispersion analysis. The alias field is yielded by collocating Eq. (20) in each node of the unit cell. The assumption of different amplitudes is introduced because the equation of equilibrium is different for each node. The analysis yields the relative wave amplitudes and the dispersion relation under which the alias field may propagate. In each element the alias field will be

$$\tilde{p}^a = \sum N_{S,i} \tilde{p}_i \tag{64}$$

where: $\tilde{p}_i$, the values of Eq. (20) at the nodes; $N_{S,i}$, the element shape functions.

Finally we must remark that the dispersion analysis can be alternatively performed characterizing the plane harmonic wave by the displacement potential. Obviously, in that case, we obtain the same results.

3 ACOUSTIC CAVITY MODES

3.1 Introduction

It is well known that the reflection of waves from boundaries or from other discontinuities creates an interference field that, if composed solely of waves of frequency equal to a natural frequency of the system, takes the form of a stationary wave field which is a natural mode of the continuum system [22]; therefore, if a finite volume of compressible fluid is bounded by the motionless and reflecting walls of a cavity it can oscillate according to stationary waves called acoustic modes. In this

section we approach the subject of the acoustic modes in three-dimensional cavities which have no analytical solution and will be solved by the finite element method.

In order to conveniently pose an algebraic eigenvalue problem, the acoustic field will be characterized by the displacement potential. Then, inserting Eq. (8) into Eq. (10), the governing equation of the discretized fluid medium will be

$$(\mathbf{K} - \omega^2 \mathbf{M})\boldsymbol{\psi} = \boldsymbol{\Theta}\mathbf{u}_N \tag{65}$$

where: $\boldsymbol{\psi}$, column matrix containing the nodal values of displacement potential.

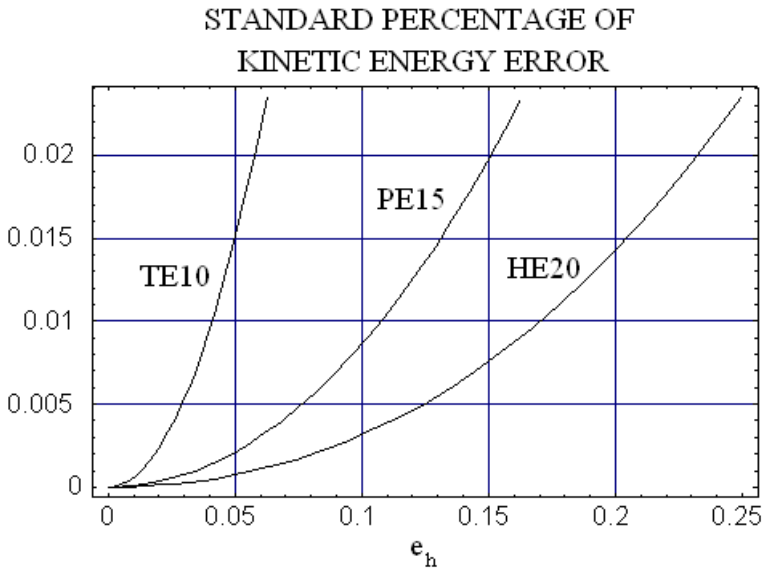

Figure 12: Standard percentage of kinetic energy error versus percentage of higher order kinetic energy.

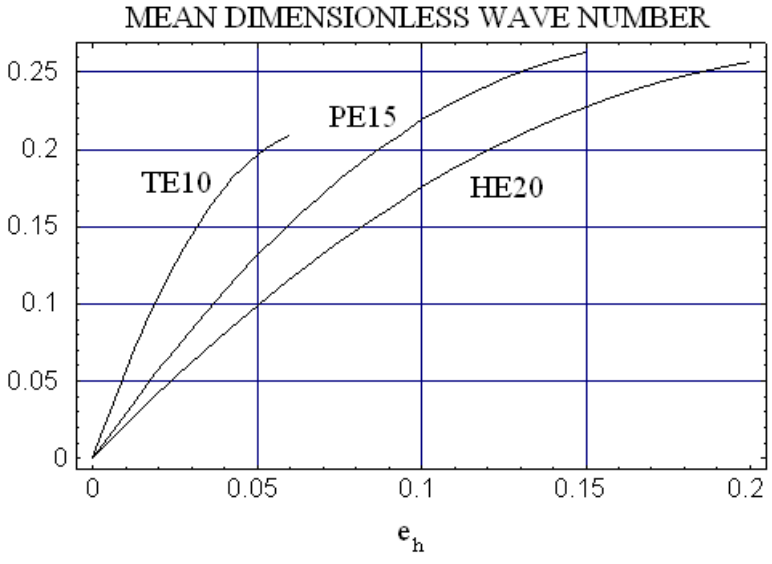

Figure 13: Mean dimensionless wave number versus percentage of higher order kinetic energy.

By considering the homogeneous part of Eq. (65) and assuming stationary waves, it is produced the so called generalized eigenproblem [23],

$$\mathbf{K}\tilde{\boldsymbol{\psi}}_j = \lambda_j \mathbf{M}\tilde{\boldsymbol{\psi}}_j \tag{66}$$

where: $\lambda_j = \omega_j^2$, the *j*-eigenvalue; $\tilde{\boldsymbol{\psi}}_j$, the *j*-eigenvector.

It is well known that the eigenvalue can be physically interpreted as the square of the natural frequency of the discretized fluid medium. The eigenvector and the element interpolation functions shape the finite element mode. Obviously, as the finite element mesh is refined and discretization error decreases, both the finite element eigenvalues and the finite element modes must converge to the eigenvalues and the eigenfunctions associated with the differential governing equation and its boundary conditions [24].

The kernel of the global stiffness matrix **K** is of dimension 1; therefore, this matrix is positive semidefinite. The generalized eigenproblem Eq. (66) has been solved by the subspace iteration method [23]. The algorithm requires that **K** be nonsingular. This restriction can be met by using an eigenvalue shift [25].

An important relation fulfilled by the eigenvectors is that of **M**-orthonormality,

$$\tilde{\boldsymbol{\psi}}_i^T \mathbf{M}\tilde{\boldsymbol{\psi}}_j = \delta_{ij} \tag{67}$$

where δ_{ij} is the Kronecker delta.

Premultiplying Eq. (66) by $\tilde{\boldsymbol{\psi}}_i^T$ and using Eq. (67), it is produced

$$\tilde{\boldsymbol{\psi}}_i^T \mathbf{K}\tilde{\boldsymbol{\psi}}_j = \delta_{ij}\omega_j^2 \tag{68}$$

If the acoustic field is characterized by the displacement potential, by Eq. (8) and (16) the modal kinetic energy of the discretized fluid medium will be

$$\overline{E}_k = \frac{1}{4}\rho\omega^2 \tilde{\boldsymbol{\psi}}^T \mathbf{K}\tilde{\boldsymbol{\psi}} \tag{69}$$

By introducing the decomposition in Eq. (15) into Eq. (69) we obtain both the basic and higher order modal kinetic energy. The latter component will be

$$\overline{E}_{kh} = \frac{1}{4}\rho\omega^2 \tilde{\boldsymbol{\psi}}^T \mathbf{K}_h \tilde{\boldsymbol{\psi}} \tag{70}$$

Finally, by introducing Eq. (68) into Eq. (69), the following expression for the modal kinetic energy it is produced

$$\overline{E}_k = \frac{1}{4}\rho\omega^4 \tag{71}$$

3.2 Numerical research

In this section it is investigated the application of the percentage of higher order kinetic energy as an error indicator for the acoustic modes computed by the finite element method. This percentage will be evaluated by Eq. (69) and (70),

$$PHE = \frac{\overline{E}_{kh}}{\overline{E}_k} \tag{72}$$

An estimation of the error for the natural frequencies and modal displacement potentials obtained with the discretized fluid domain will be presented. The reference model will be obtained by dividing each element of the actual mesh into eight elements.

The modal displacement potentials obtained with the actual model and the ones obtained with the reference model will be compared by the modal kinetic energy error

$$KEE = \frac{\overline{E}_k - \overline{E}_k^{REF}}{\overline{E}_k^{REF}} \tag{73}$$

where $\overline{E}_k$ and $\overline{E}_k^{REF}$ are defined by Eq. (69).

By considering Eq. (71), the modal kinetic energy error Eq. (73) can be evaluated as

$$KEE = \left(\frac{\omega}{\omega^{REF}} \right)^4 - 1 \tag{74}$$

Obviously, from Eq. (74) the natural frequency error is inferred.

In order to investigate the behaviour of the percentage of higher order kinetic energy as a modal error indicator, the application of the standard correlation, yielded by the numerical dispersion analysis, between the percentage of higher order kinetic energy and the kinetic energy error, Eq. (60) to (62), is explored. The kinetic energy error computed by the above correlation from the percentage of higher order modal kinetic energy associated with the actual model will be called the standard modal kinetic energy error, SKEE. This standard error will be compared with the one computed by Eq. (74). Two acoustic cavities will be analyzed: a tapered cavity discretized by HE20 element, Fig. 14; and a half of pyramidal cavity discretized by TE10 element, Fig. 15. The results are shown in Tables 4 and 5, respectively.

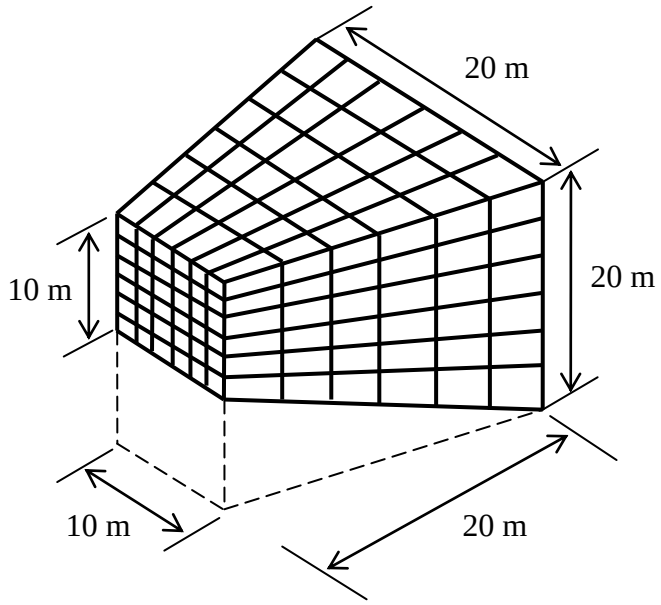

Figure 14: Tapered cavity. Sound velocity, c = 346 m/s.

From Tables 4 and 5, it is observed that both the percentage of higher order kinetic energy Eq. (72) and the kinetic energy error Eq. (74) increase with the modal order. The percentage of higher order kinetic energy decreases as the mesh is refined. Clearly, the numerical research reveals that the percentage of higher order kinetic energy behaves as

a modal error indicator. This result is consistent with the one obtained by the numerical dispersion analysis carried out for harmonic waves.

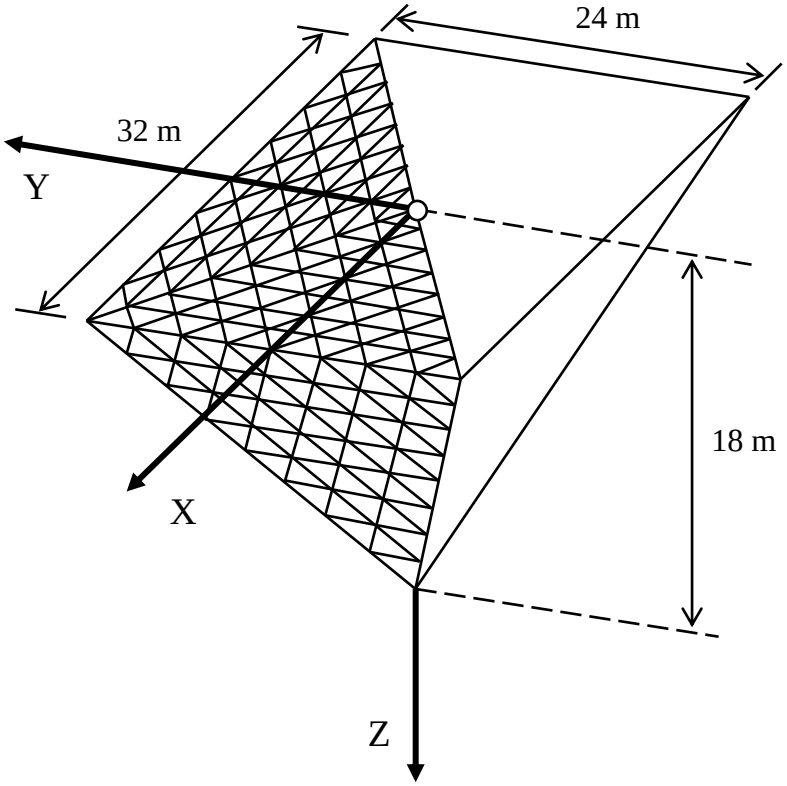

Figure 15: Half of pyramidal cavity. Sound velocity, c = 346 m/s.

From Tables 4 and 5, and Fig. 16 and 17, it is observed that the standard error SKEE generally overestimates the modal kinetic energy error KEE, Eq. (74), at least in the interested range of error. Typically it is considered that a kinetic energy error around one per cent is an optimum upper bound to properly capture the acoustic modes, at least from the engineering point of view. In this case, the natural frequency error would be negligible. It can be observed that by the standard error SKEE the corresponding cutoff modal order can be properly captured. As a final remark, a one per cent of kinetic energy error roughly corresponds to six elements per wavelength for TE10 element, and between four and five elements per wavelength for HE20 element, Fig. 12 and 13. In this case, from Tables 1 and 3, it can be inferred that the effect of the spatial discretization over the group velocity and therefore over the wave velocity is negligible.

4 CONCLUSIONS

This paper studies the propagation of time-harmonic acoustic waves in fluid media discretized by energy-orthogonal finite elements. In this formulation the element stiffness matrix is split into basic and higher order components which are related to the mean and deviatoric components of the gradient of acoustic pressure, respectively. This decomposition is applied both to the stiffness matrix and to the kinetic energy of the finite element assemblage. The research is focused on the properties of the higher order kinetic energy as an error indicator. The noteworthy conclusions of this paper are:

- By numerical dispersion analysis of plane harmonic waves a standard correlation between percentage of higher order kinetic energy and kinetic energy error is yielded. The above correlation is highly dependent of the considered element.
- The standard correlation is used as a reference to apply the percentage of higher order kinetic energy as an error indicator for the acoustic cavity modes computed by the finite element method. Typically it is considered that a kinetic energy error around one per cent is an optimum upper bound to properly capture the acoustic modes. The numerical research reveals that by the standard correlation the modal kinetic energy error is generally overestimated in the interested error range, and a cutoff modal order can be properly selected.

The application of the proposed procedure to more complex waves and media is subject of research.

MODE	FR REF Hz	PEH REF	PEH	KEE	SKEE
1	8.367348	0.005253	0.020643	0.000213	0.000120
2	10.254183	0.005863	0.023076	0.000181	0.000150
3	10.723037	0.006894	0.027061	0.000270	0.000208
4	13.900437	0.012186	0.047503	0.000244	0.000661
5	15.248240	0.014688	0.056427	0.001358	0.000944
6	16.185534	0.013126	0.050982	0.000460	0.000765
7	17.653668	0.021225	0.081510	0.002510	0.002040
8	19.383300	0.025091	0.094649	0.003049	0.002799
9	19.625853	0.023625	0.089744	0.001444	0.002500
10	19.661165	0.024308	0.092719	0.002912	0.002679
11	21.216222	0.028169	0.106661	0.002819	0.003612
12	21.777377	0.029530	0.111531	0.002592	0.003974
13	21.955504	0.030879	0.116365	0.003246	0.004353
14	22.166654	0.027799	0.104825	0.001992	0.003480
15	24.842269	0.036216	0.134124	0.004083	0.005917
16	25.251863	0.046891	0.171357	0.010896	0.010112
17	25.989087	0.045434	0.164372	0.010063	0.009226
18	26.399584	0.043411	0.160458	0.004899	0.008750
19	27.144879	0.042850	0.156726	0.005206	0.008310
20	27.919302	0.051046	0.183629	0.009410	0.011785
21	28.007702	0.046622	0.170426	0.008902	0.009991
22	28.312110	0.052364	0.189307	0.011058	0.012609
23	29.157168	0.056376	0.205599	0.013495	0.015160
24	29.295293	0.048908	0.171845	0.006822	0.010176
25	29.454904	0.051953	0.192371	0.012197	0.013068
26	29.963084	0.055955	0.202152	0.011436	0.014597
27	30.800392	0.053507	0.193305	0.008889	0.013210
28	31.240025	0.063252	0.226136	0.014250	0.018776
29	31.575416	0.050851	0.179857	0.007838	0.011255
30	32.278370	0.063521	0.214050	0.016066	0.016592

Table 4: Estimation of the modal discretization error for a tapered cavity.

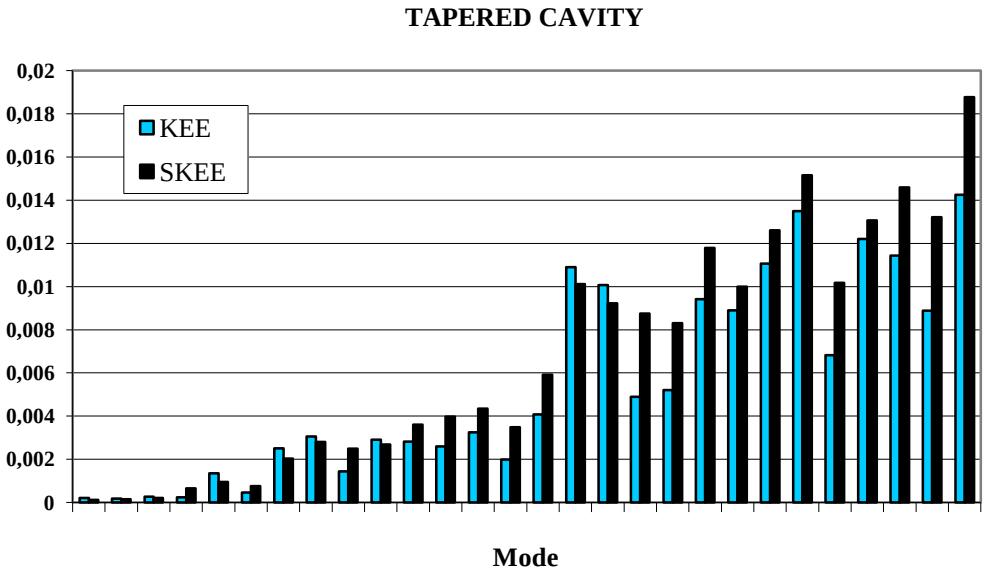

Figure 16: Standard modal kinetic energy error SKEE versus modal kinetic energy error KEE for a tapered cavity.

MODE	FR REF Hz	PEH REF	PEH	KEE	SKEE
1	7.742879	0.001256	0.004498	0.000328	0.000119
2	10.924825	0.003408	0.012184	0.000586	0.000874
3	11.245958	0.003474	0.012425	0.000520	0.000909
4	14.935495	0.006377	0.022751	0.002579	0.003063
5	16.378355	0.008045	0.028249	0.005197	0.004735
6	18.695083	0.009152	0.031975	0.006154	0.006076
7	20.527646	0.011413	0.039084	0.008533	0.009108
8	20.816339	0.012021	0.041525	0.007681	0.010293
9	21.655237	0.011962	0.041286	0.006978	0.010173
10	22.553624	0.014465	0.049086	0.012879	0.014432
11	23.969180	0.017444	0.059538	0.015512	0.021333
12	25.862455	0.019508	0.064886	0.020359	0.025399
13	26.730454	0.017795	0.060549	0.014438	0.022074
14	26.918635	0.021915	0.074262	0.023056	0.033410
15	28.492760	0.023006	0.078155	0.023469	0.037070
16	29.274352	0.024027	0.079723	0.028826	0.038599
17	30.061341	0.026414	0.085174	0.033624	0.044166
18	31.121104	0.026708	0.088292	0.029118	0.047525
19	31.339265	0.026567	0.086435	0.032736	0.045509
20	31.604209	0.027741	0.090491	0.032800	0.049971

Table 5: Estimation of the modal discretization error for a half of pyramidal cavity.

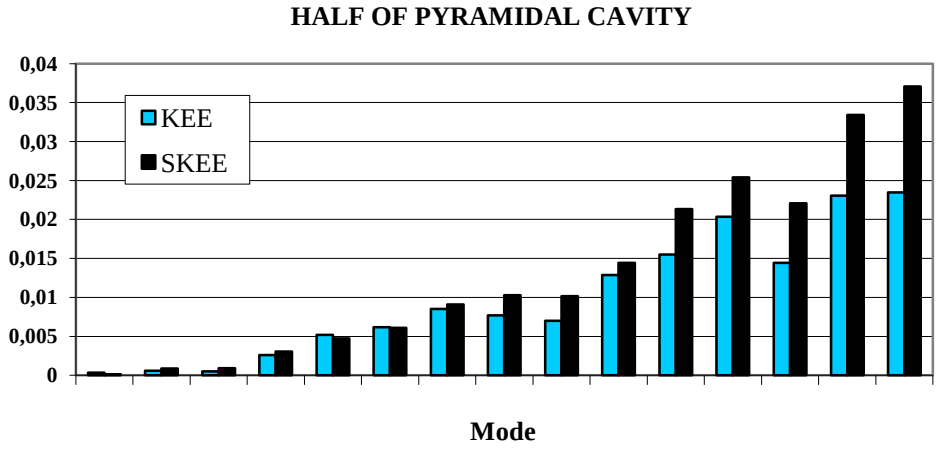

Figure 17: Standard modal kinetic energy error SKEE versus modal kinetic energy error KEE for a half of pyramidal cavity.

REFERENCES

[1] H.L. Schreyer, Dispersion of semidiscretized and fully discretized systems. T. Belytschko, T.J.R. Hughes eds. *Computational methods for transient analysis*. Elsevier Science, 1983.

[2] I. Harari, Dispersion, pollution and resolution. S. Marburg, B. Nolte eds. *Computational acoustics of noise propagation in fluids*. Springer, 2008.

[3] L.M. Brekhovskikh, Yu.P. Lysanov, *Fundamentals of ocean acoustics*. Springer, 2003.

[4] S. Marburg, B. Nolte, A unified approach to finite and boundary element discretization in linear time-harmonic acoustic. S. Marburg, B. Nolte eds. *Computational acoustics of noise propagation in fluids*. Springer, 2008.

[5] F. Ihlenburg, *Finite element analysis of acoustic scattering*. Springer, 1998.

[6] D. Givoli, Computational absorbing boundaries. S. Marburg, B. Nolte eds. *Computational acoustics of noise propagation in fluids*. Springer, 2008.

[7] C.A. Felippa, B. Haugen, C. Militello, From the individual element test to finite element templates: evolution of the Patch Test. *International Journal for Numerical Methods in Engineering*, **38**, 199-229, 1995.

[8] P.G. Bergan, M.K. Nygärd, Finite elements with increased freedom in choosing shape functions. *International Journal for Numerical Methods in Engineering*, **20**, 643-664, 1984.

[9] C.A. Felippa, A survey of parametrized variational principles and applications to computational mechanics. *Computer Methods in Applied Mechanics and Engineering*, **113**, 109-139, 1994.

[10] F.J. Brito Castro, Dispersion analysis of gravity waves in fluid media discretized by energy-orthogonal finite elements. *International Journal for Computational Methods in Engineering Science and Mechanics*, **15**, 499-511, 2014.

[11] O.C. Zienkiewicz, R.L. Taylor, *The finite element method, Vol. 1*. Butterworth-Heinemann, 2000.

[12] D. Royer and E. Dieulesaint, *Elastic waves in solids, Vol. 1*. Springer, 2000.

[13] M. Okrouhlík, C. Höschl, A contribution to the study of dispersive properties of one-dimensional lagrangian and hermitian elements. *Computers and Structures*, **49**, 779-795, 1993.

[14] R.A. Horn and C.R. Johnson, *Matrix analysis*. Cambridge University Press, 1992.

[15] W.H. Press, S.A. Teukolsky, W.T. Vetterling and B.P. Flannery, *Numerical recipes in fortran*. Cambridge University Press, 1992.

[16] R.B. King, *Beyond the quartic equation*. Birkhäuser, 1996.

[17] Z-Q. Qu, *Model order reduction techniques: with applications in finite element analysis*. Springer, 2004.

[18] L. Brillouin, *Wave propagation in periodic structures*. Dover Publications, 2003.

[19] J.D. Achenbach, *Wave propagation in elastic solids*. Elsevier, 1975.

[20] J. Barlow, More on optimal stress points-reduced integration, element distortions, and error estimation. *International Journal for Numerical Methods in Engineering*, **28**, 1487-1504, 1989.

[21] R.H. MacNeal, *Finite elements: their design and performance*. Marcel Dekker, 1994.

[22] F.J. Fahy, *Sound and structural vibration: radiation, transmission and response*. Academic Press, 1985.

[23] K.J. Bathe, *Finite element procedures*. Prentice Hall, 1996.

[24] J.N. Reddy, *Applied functional analysis and variational methods in engineering*. Krieger Publishing Company, 1986.

[25] R.D. Cook, D.S. Malkus, and M.E. Plesha, *Concepts and applications of finite element analysis*. John Wiley, 1989.